Tribology Letters (2018) 66:55
https://doi.org/10.1007/s11249-018-1003-4

ORIGINAL ARTICLE

Characterization of the Tribological Behavior of the Textured Steel Surfaces Fabricated by Photolithographic Etching

Yufu Xu[1] · Jingyuan Yu[1] · Jian Geng[1] · Rasha Abuflaha[2] · Dustin Olson[2] · Xianguo Hu[1] · Wilfred T. Tysoe[2]

Received: 16 October 2017 / Accepted: 19 February 2018 / Published online: 1 March 2018

Abstract
A photolithography etching technique was used to fabricate textured surfaces on steel samples. The friction and wear behavior of the textured surfaces were studied with surface contact sliding. The influence of the diameter and the density of the dimples were investigated. The results show that the textured surfaces with appropriate diameters and densities had excellent friction reducing and antiwear properties. Large-diameter dimples can destroy the integrity of the lubricating film, and low- or high-density dimples produce more iron sulfates and fewer ferrous sulfides on the rubbing surfaces due to the tribo-reactions, which resulted in higher friction coefficients. The tribo-chemical films, oil micro-reservoir and wear debris-containing roles of the dimples together help the textured surfaces to provide improved antiwear properties.

Keywords Textured steel surfaces · Laser surface texturing · Photolithographic etching · Friction and wear behavior

1 Introduction

Control of the friction and wear of the friction pairs is an important issue in mechanical engineering in order to save energy, reduce emission and enhance the efficiency of machines. Surface texturing has been considered to be an effective friction- and wear-reducing technology over the last two decades [1]. Many workers including Etsion [2–4] and others [5–8] have carried out extensive work on surface texturing, both theoretically and experimentally, and they found that the texture shape, dimple diameter, density and ratio of diameter/depth could affect the tribological behavior. Dimples can operate by creating additional load-bearing capacity [9], but it has also been proposed that under starved conditions they can also function by providing lubricant micro-reservoirs [10] or by trapping wear debris [11].

Besides having good antifriction and antiwear properties, the textured surfaces can also prolong wear life and improve fuel efficiency of internal combustion engines [12]. However, not all the textured surfaces have a positive effect and the rules are different with the variation of the lubrication regime [13], and how to precisely obtain desired tribological performances via surface textures is a problem still remaining unsolved [14].

Most textured surfaces are made by laser ablation [15–18], known as laser surface texturing (LST), but it is difficult to make textured surfaces on parts with complex morphologies, and requires expensive equipment, while other techniques such as machining [19], ion beam texturing [20] and photolithographic etching have been used. However, the accumulation of the metallic debris adjacent to the dimples during the laser processing requires a secondary polishing treatment to remove it. Therefore, simpler methods for preparing textured steel surfaces are needed.

Among these techniques, photolithographic etching has been a commonly used method to fabricate well-defined structures on surfaces in the semiconductor industry for more than 50 years [21]. There are several advantages to this method. First, compared with traditional laser texturing, this approach is much easier to implement and requires relatively simple equipment. Second, it can be used to fabricate dimples with a wide range of shapes and distributions, has a deep etching capability, and a relatively expeditious transition from optical design to device fabrication and can also be employed in texturing steel surfaces [22]. Finally, it obviates the need for a final polishing step to remove laser ablation

✉ Yufu Xu
xuyufu@hfut.edu.cn

[1] Institute of Tribology, School of Mechanical Engineering, Hefei University of Technology, Hefei 230009, China

[2] Department of Chemistry and Biochemistry and Laboratory for Surface Studies, University of Wisconsin-Milwaukee, Milwaukee 53211, USA

debris. Zhang and Meng [23] used photochemical machining to fabricating microstructures on carbon steel surfaces. The influence of the parameters of photolithography and wet chemical etching was investigated, and they provided a method for precisely controlling the textured morphologies. While steel surfaces have been textured by photolithographic etching, there are few reports [24, 25] on their tribological behavior. In addition, to our understanding one of the main roles of the textured surfaces, namely micro-reservoirs for lubricant and micro-traps for wear debris, is still far from complete. In particular, little work covers the effects of the tribo-film on the etched textured surfaces. As is known, the tribo-film plays an important lubricating role under boundary lubrication regime. Therefore, the corresponding lubricating mechanism of the textured surfaces with photolithographic etching is worthy of being clarified.

In the present work, we fabricated a series of textured dimples on steel surfaces using photolithographic etching and studied their friction and wear behavior under oil-lubricated conditions in boundary lubrication regime. The influence of dimple diameter and density was investigated, and the corresponding mechanisms were also revealed.

2 Experimental

2.1 Materials

The substrate was a SAE1020 steel plate with dimensions of 25.4 mm × 25.4 mm × 1.57 mm (height), and its surface roughness R_a was 0.75 μm before texturing. The pin was made of SAE1045 steel and polished to obtain a surface roughness $R_a \leq 0.05$ μm. The lubricating oil was L-AN32 machine oil purchased from Sino Petroleum Corp. with the viscosity being 32 cSt at 40 °C. The oil is composed of liquid mixtures of hydrocarbons and some (< 0.5%) additives containing sulfur.

2.2 Surface Texturing Process

Shipley S1813 photoresist was spun on the SAE1020 steel plate at speed of 300 rpm for 10 s, 900 rpm for 10 s and 4000 rpm for 60 s, respectively. After that, the coated plate was baked at 115 °C for 2 min and shapes with desired sizes, distributions and separations were patterned using a printed mask, exposed to ultraviolet radiation with 365 nm for 30 min. According to the previous literature [26] and the potential industrial applications, the diameter of the dimples is designed to vary from 400 to 800 μm, and the density of the dimples varies from 2.5 to 18% with the change of the masks. The masks were facilely fabricated by printing an image of the mask dimple pattern onto a transparency using a high-resolution (1200 dpi) laser printer. Then, the coating was baked at 120 °C for 6 min and developed using MF-321 developer for 3 min and washed with deionization water. After being heated at 115 °C for 2 min, the plate was etched by immersion in a 3% dilute nitric acid solution for 10 min. The plate was then washed in an acetone solution to remove any remaining photoresist and finally dried. The densities of the dimples vary from 2.5, 7 to 18%. Note that the depths of the dimples can be varied by adjusting the etching time, although this was not investigated as part of this work.

2.3 Tribological Tests

The tribological tests were carried on a CFT-I tribometer (Lanzhou Zhongke Kaihua Technology Development Co., LTD) in a pin-on-plate reciprocating sliding mode. The steel pin and plate were lubricated by L-AN32 machine oil, and the detailed testing conditions are listed in Table 1. The choice of friction test conditions is based on both the test range of the experimental instrument and the potential application field of the textured surfaces. About 0.5 mL oil was added on the surface, and the frequency of the reciprocating tests was 5 Hz. The diameter of the pin was 5 mm. The nominal contact pressure is 5.1 MPa. The tribo-test for each set of textures was repeated twice. After sliding, the friction pairs were washed in acetone. The friction coefficients were recorded automatically by the instrument from the ratio of friction force to the normal load. The wear volumes were calculated from the product of the area of the wear cross section and stroke length.

2.4 Characterization

The rubbed surfaces were imaged with a VK-X100 3D laser scanning microscope (Keyence, Japan) to obtain 2D and 3D optical micrographs and surface profiles of the worn surfaces on the steel plate. The chemical states of the typical elements on the surfaces around the dimples after sliding were characterized using an ESCALAB 250 X-ray photoelectron spectrometer (XPS, Thermo Scientific, USA) with Al Kα radiation. The components of the XPS profiles were fit using Origin software by Gaussian fitting function.

Table 1 Tribological testing conditions

Testing conditions	Value
Stroke length/mm	5
Testing temperature/ °C	25–27
Sliding velocity/mm·s^{-1}	50
Normal load/N	100
Duration/min	80

3 Results and Discussion

3.1 Influence of Diameter of the Dimples

Figure 1 shows optical images of untextured (Fig. 1a) and textured surfaces (Fig. 1b–d) with different diameters. It can be seen that the dimples are uniformly distributed on the surfaces and the center-to-center spacing of the dimples was 2 mm. The samples can be used directly without further polishing, indicating the successful preparation of the textured surfaces with photolithography etching method.

Figure 2a presents the variation in friction coefficient with sliding time. In the run-in stage (first 30 min), there were no clear differences between the friction coefficients of the different samples. At longer time, the textured surfaces with small-diameter dimples (TSD, 400 μm) and the textured surfaces with medium-diameter dimples (TMD, 600 μm) had a relatively lower friction than the untextured surfaces (UT). However, the textured surfaces with large-diameter dimples (TLD, 800 μm) had a higher friction coefficient than the UT. These results are shown clearly in Fig. 2b, which shows the average friction coefficient during the stable sliding stage between 30 and 80 min. These results confirm the same conclusion from previous laser surface texturing that not all the textured surfaces have the

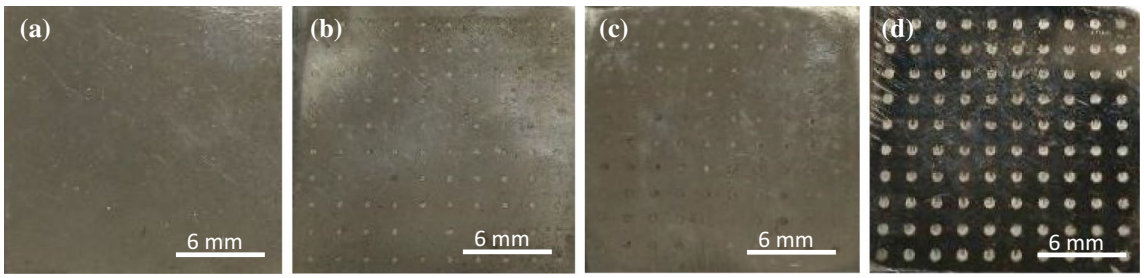

Fig. 1 Optical photographs of untextured (**a**) and textured surfaces with different diameter: 400 μm (**b**), 600 μm (**c**) and 800 μm (**d**)

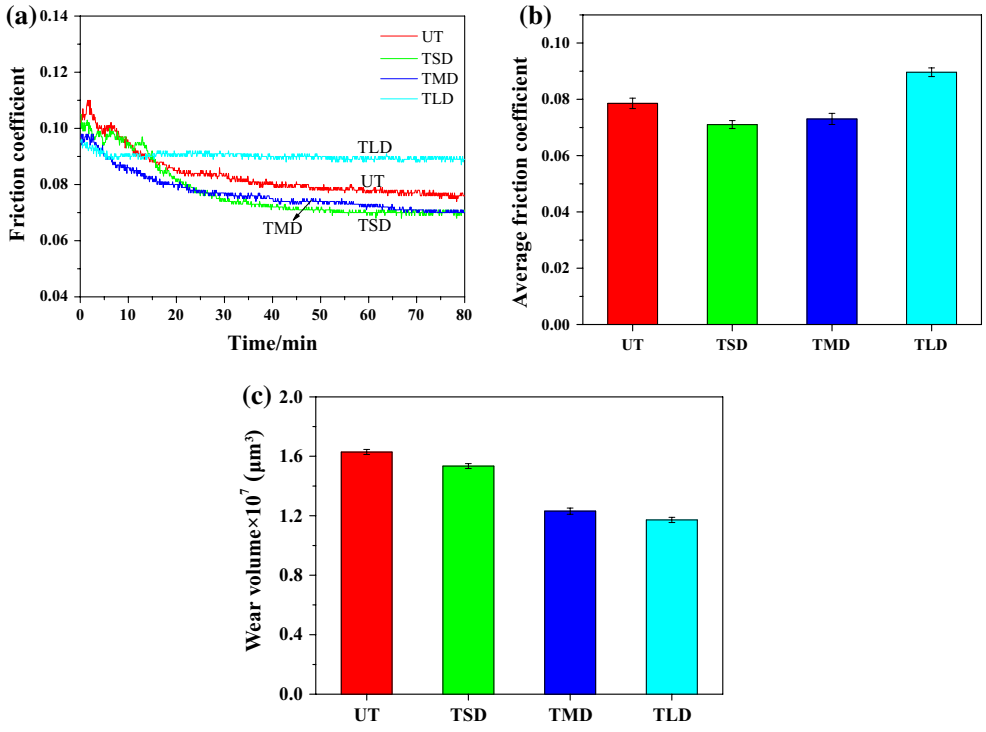

Fig. 2 Influence of the diameter of the dimples on the friction coefficient (**a**), average friction coefficient of stable sliding stage (**b**) and wear volume (**c**)

superior antifriction roles, and too large dimples might be harmful for the friction reduction effects.

The wear volumes of the untextured and textured surfaces with different dimples are shown in Fig. 2c. All the textured surfaces had lower wear volumes than the UT sample. Comparing with the wear volume of the UT surface, those with TSD, TMD and TLD decreased by 6 ± 0.2, 24 ± 0.4 and 28 ± 0.1%, respectively, suggesting that surfaces textured by photolithographic etching improved the antiwear performance [24].

Figure 3 shows 2D optical micrographs and surface profiles of the untextured area of the worn surfaces of the steel plates. There is a wide and deep worn band on the untextured surfaces. With an increase in diameter of the dimples, the worn region becomes narrower and shallower,

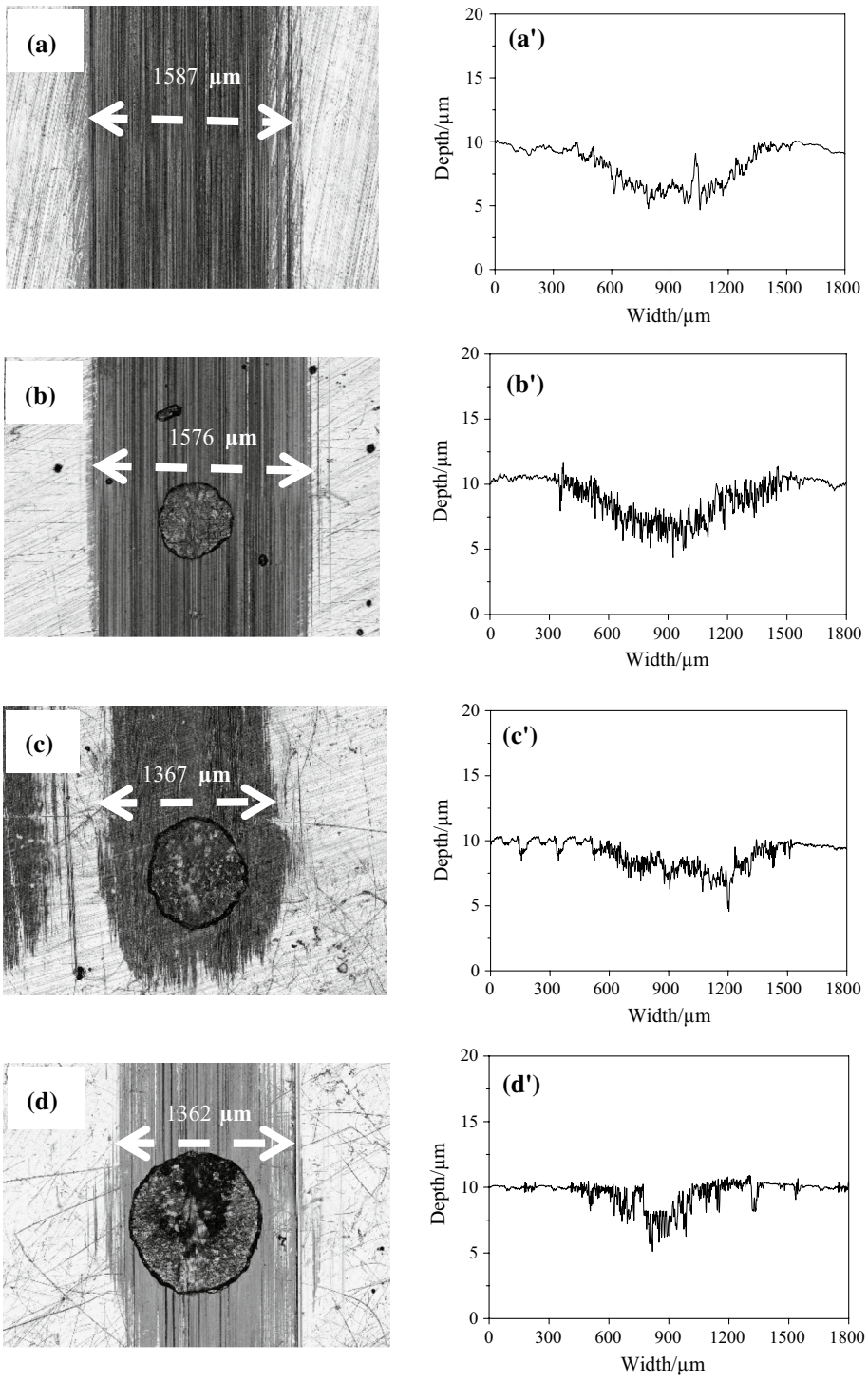

Fig. 3 2D optical micrographs (**a**–**d**) and surface profiles (**a′**–**d′**) of the untextured area of the worn surfaces: UT (**a**, **a′**), TSD (**b**, **b′**), TMD (**c**, **c′**) and TLD (**d**, **d′**)

resulting in lower wear volumes. These results agree well with those shown in Fig. 2c.

Figure 4 shows 3D optical micrographs and surface profiles of the textured areas of the worn surfaces of the steel plates. The green and blue colors show a deep wear scar on the untextured surface in Fig. 4a. In addition, as shown in Fig. 4b–d, b′–d′, an increase in the diameter of the dimples increased their depth on the worn surfaces, indicating

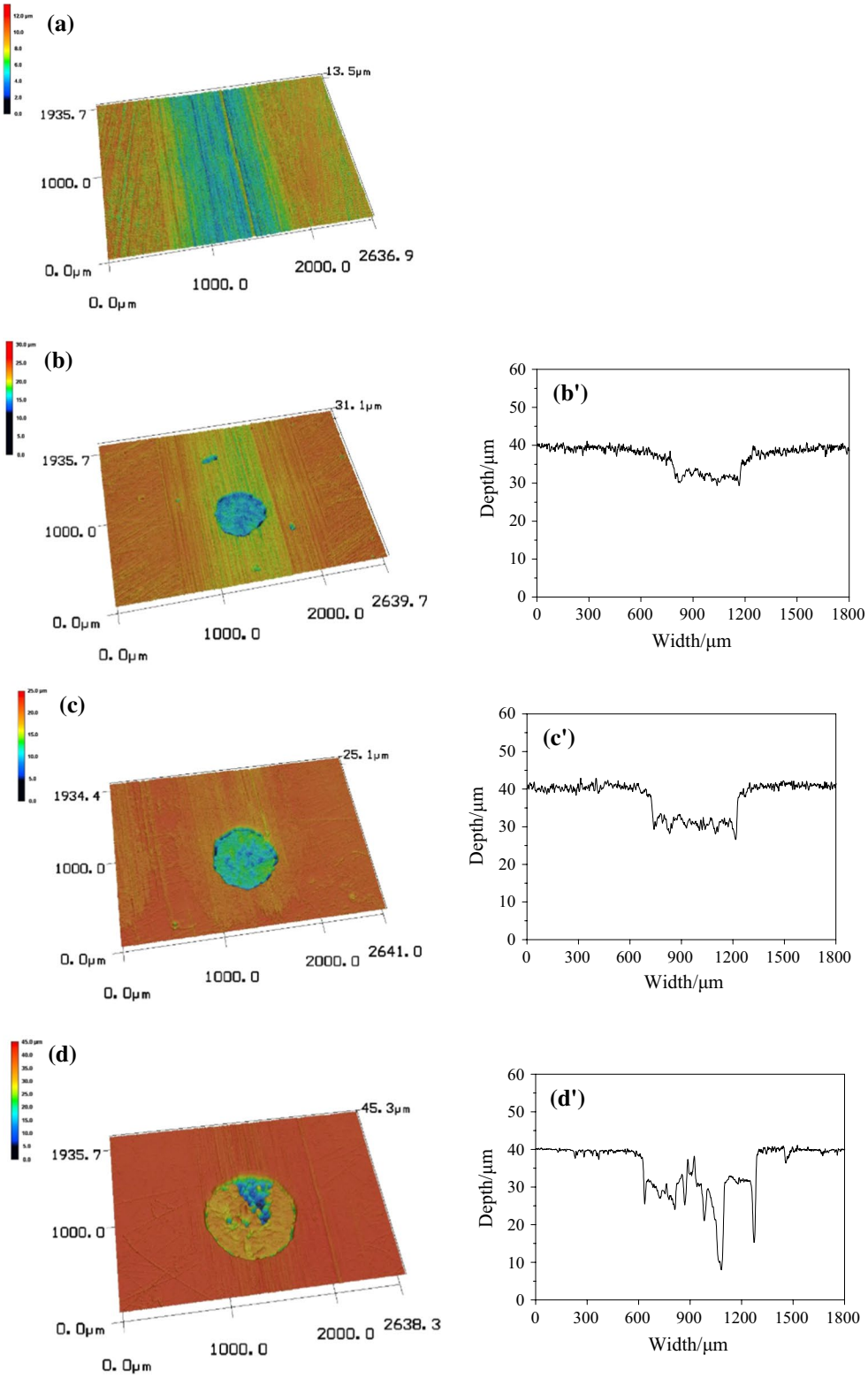

Fig. 4 3D optical micrographs (**a**–**d**) and surface profiles (**b**′–**d**′) of the textured area of the worn surfaces of the steel plates: UT (**a**), TSD (**b**, **b**′), TMD (**c**, **c**′) and TLD (**d**, **d**′)

reduced wear [27]. Considering these results and the high friction coefficients of the surfaces with large dimples, the textured surfaces with medium-diameter dimples were chosen for further investigation.

3.2 Influence of Density of the Dimples

The optical photographs of three kinds of textured surfaces with the same medium diameters, but different densities are displayed in Fig. 5. The density of the dimples can be easily controlled by fabricating different masks [28], which emphasized one of the advantages of this method. Three kinds of textured surfaces with low-density dimples (TSLD), textured surfaces with medium-density dimples (TMD) and textured surfaces with high-density dimples (TSHD) were compared with the UT surface.

Figure 6 shows the influence of dimple density on the friction coefficient and wear volume of the plates. All the textured surfaces had lower wear volumes than the UT surface, suggesting good antiwear properties of the textured surfaces. Low or high dimple densities did not help reduce the wear or increase the friction coefficient of the textured surfaces. This is possibly because low dimple densities cannot provide adequate oil reservoirs [29], while high dimple densities might destroy the integrity of the lubricating oil film [30]. As is known, high dimple densities can result in a decrease in the real contact area and an increase in the real contact pressure, which makes a thinner oil film between the

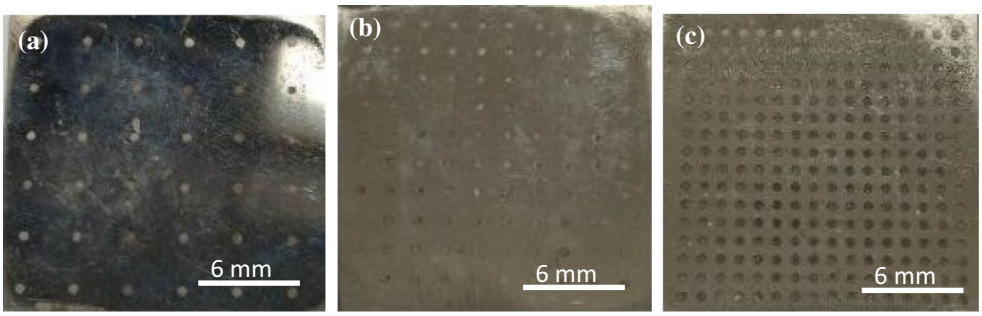

Fig. 5 Optical photographs of textured surfaces with different density: TSLD (**a** 2.5%), TMD (**b** 7%) and TSHD (**c** 18%)

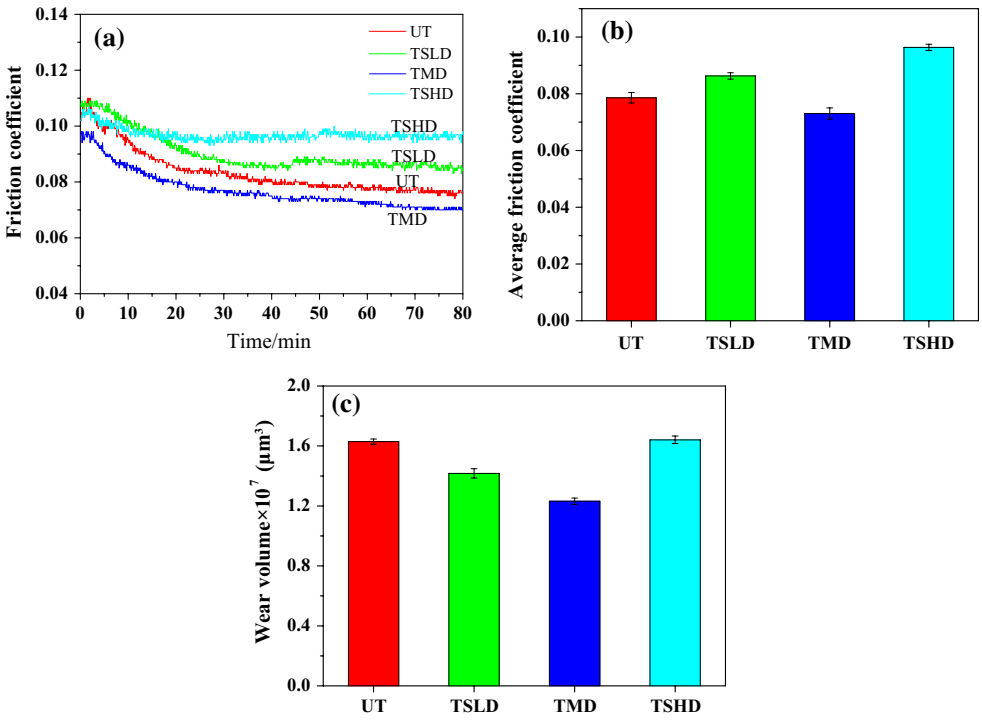

Fig. 6 Influence of the density of the dimples on the friction coefficient (**a**), average friction coefficient of stable sliding stage (**b**) and wear volume (**c**)

tribo-pairs by allowing the pressurized oil to escape from the contact area. When the thickness of the oil film is less than the surface roughness, it can be regarded as the oil film not being complete, that is, the integrity of the lubricating oil film is destroyed.

Figure 7 shows 2D optical micrographs and surface profiles of the untextured area of the worn surfaces with different dimple densities. It only covered TSLD and TSHD, which were compared with TMD and UT. The surfaces with low and high dimple densities formed wider and deeper wear scars, agreeing well with the results shown in Fig. 6c.

Figure 8 shows steel plates with different dimple densities. The dimple depth of the TSLD was lower than that of the TMD, which was in accord with the previous results, while the TSHD showed the opposite behavior, perhaps as a result of uneven wear [31] due to damage of the lubricating oil film.

3.3 Surface Chemical Analysis

The worn surfaces on the whole samples were analyzed by XPS to investigate the possibility of chemical changes occurring during sliding. As shown in Table 2, the main components on the surfaces were carbon and oxygen which may arise from either surface contamination on the steel or the organic compounds in the base oil. The proportion of iron and oxygen in the surface region is higher on textured surfaces, perhaps because of the formation of iron compounds due to tribo-reactions during wear [32]. Although there is no significant difference in the typical elements that were detected on the rubbing surfaces between photolithography etching surfaces and LST surfaces in the previous work [33], the concentration and the variation of the chemical components of the tribo-film are different. Unfortunately, it is hard to compare them due to the different sliding conditions. Under the same lubricating condition, the higher the concentration of the elements, the thicker the tribo-film. Due to the protective role of the thicker tribo-film, the textured surfaces have a lighter wear than the UT. Moreover, the detailed analysis for the main components of the tribo-film is necessary to explain their tribological behaviors.

The C1s XPS spectra of worn textured surfaces with different diameter dimples are shown in Fig. 9. They can be divided into three peaks located at ~ 288.7 (Peak 1), ~ 285.7 (Peak 2) and ~ 284.7 (Peak 3) eV, which are ascribed to COOR or carbonate, C–OH and carbon chain with C–C(H) groups [33, 34], respectively. These results indicate that the adsorbed films are composed of oxidized carbons and organics with carbon chain species, probably arising from the base oil. The peak areas reflect the content of the compounds under the same measure conditions [35]. Quantitative XPS atomic ratios can effectively reflect the chemical components in the tribo-film [36]. The larger relative peak areas of the carbon chain with C–C(H) groups in TSD and TMD samples suggest higher content of these compounds in the adsorbed films. Organics with carbon chains with C–C(H) groups have excellent adsorbing and slippery roles during sliding process. This is the direct reason for the better friction reduction effects of TSD and TMD than that of the UT. Additionally, the TLD had the lowest relative peak areas of

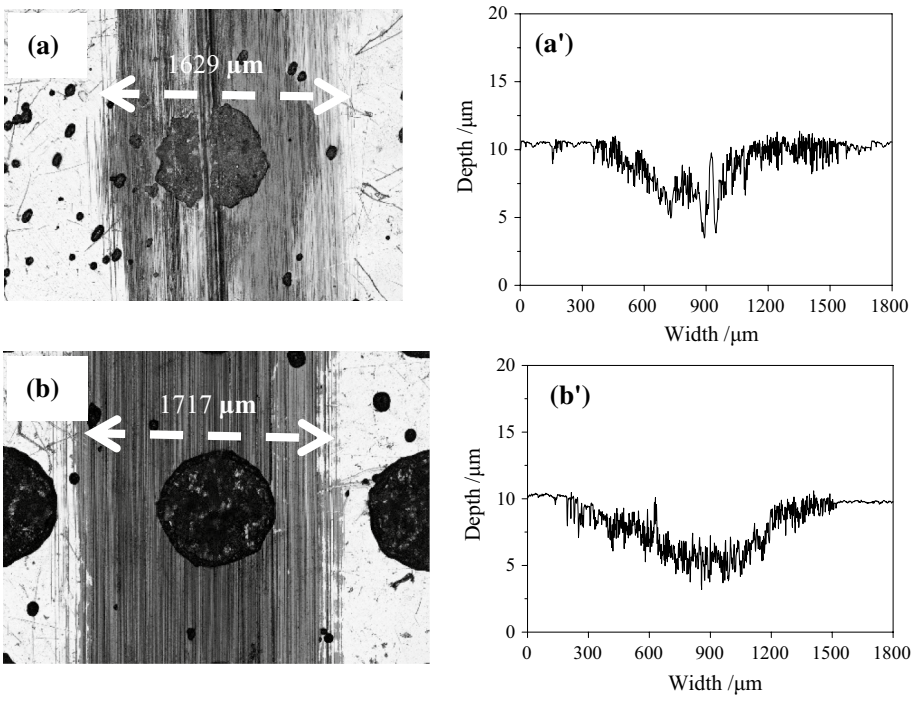

Fig. 7 2D optical micrographs (**a**, **b**) and surface profiles (**a′**, **b′**) of the untextured area of the worn surfaces with different density of the dimples: TSLD (**a**, **a′**) and TSHD (**b**, **b′**)

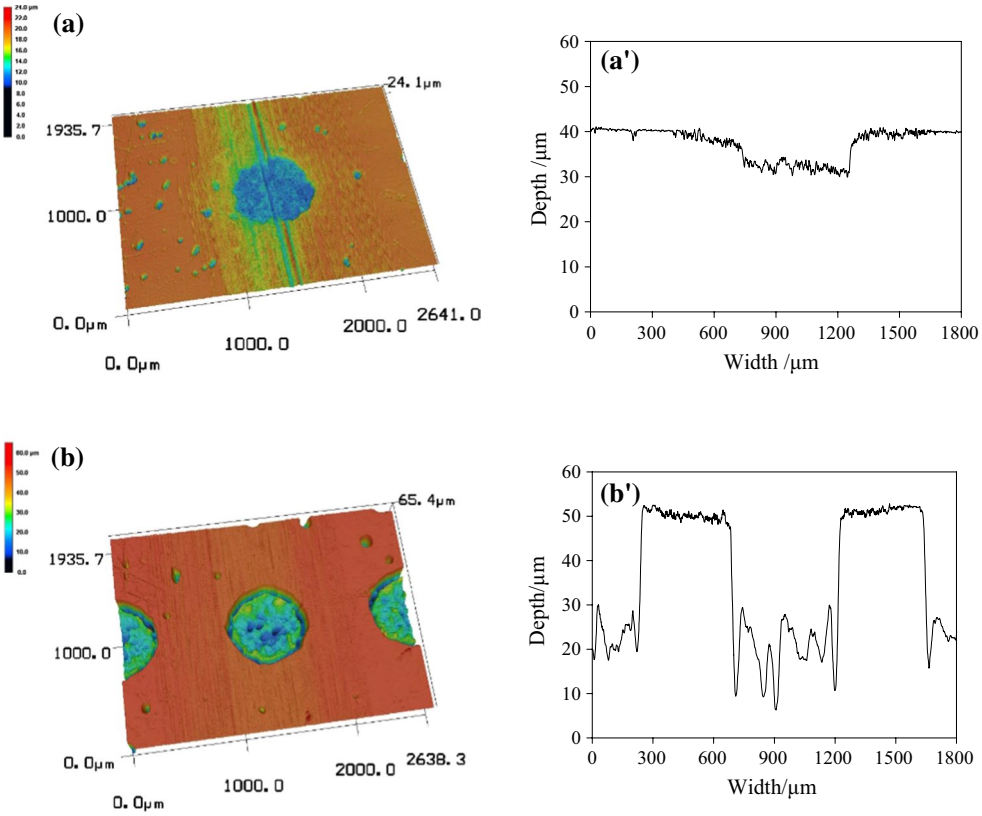

Fig. 8 3D optical micrographs (**a**, **b**) and surface profiles (**a′**, **b′**) of the textured area of the worn surfaces of the steel plates with different density of the dimples: TSLD (**a**, **a′**) and TSHD (**b**, **b′**)

Table 2 The content of typical elements on the worn surfaces with different diameter dimples obtained from the relative areas under the peaks for each element, where the atomic percentages were calculated using standard sensitivity factors incorporated into the affiliated software of the XPS instrument

The lower sample surfaces	Atomic percent (%)					
	Si	S	Mn	Fe	C	O
UT	2.36	1.46	0.86	1.98	69.43	23.91
TSD	2.61	1.54	1.03	5.15	64.23	25.44
TMD	2.21	1.1	1.27	4.52	65.76	25.13
TLD	1.88	0.59	0.39	2.45	69.9	24.29

the carbon chain with C–C(H) groups in these four surfaces; thus, it has a higher friction coefficient than the UT for the same reason.

Figure 10 shows the O1s XPS spectra of the worn textured surfaces with different diameter dimples, which can be resolved into three peaks at ~ 532.5 (Peak 1), ~ 531.8 (Peak 2) and ~ 530.8 (Peak 3) eV belonged to sulfates, hydroxides and iron oxides [37–39], respectively. The sulfur in the film arises due to reaction with sulfur-containing additive in the lubricating oil. It can be seen that the concentration of iron oxide and sulfates decreased after texturing, indicating that the oil micro-reservoir properties of the textured dimples helped to inhibit metal oxidation during sliding. In addition to this, higher concentration of the hydroxides was observed after texturing. This seems to be in contrast to the C1s results since fewer C–OH groups were measured after texturing. It can be explained by the fact that the C–OH groups in alcohols can react with the metal during sliding and form metal hydroxides, which can reduce the wear of the surfaces [40]. Although the TMD had the highest metal hydroxides (Peak 2), its antiwear performance was worse than TLD. This means that other components in the tribo-film should play an antiwear role.

Figure 11 presents the Fe2p XPS spectra of the worn textured surfaces with different diameter dimples. As can be seen, all the $Fe2p_{3/2}$ peaks can be divided into four components located at ~ 712.1 (Peak 1), ~ 711.9 (Peak 2), ~ 711.5 (Peak 3) and 710.8 (Peak 4) eV, which are proposed to correspond to ferrous sulfate, ferrous sulfide, iron hydroxide

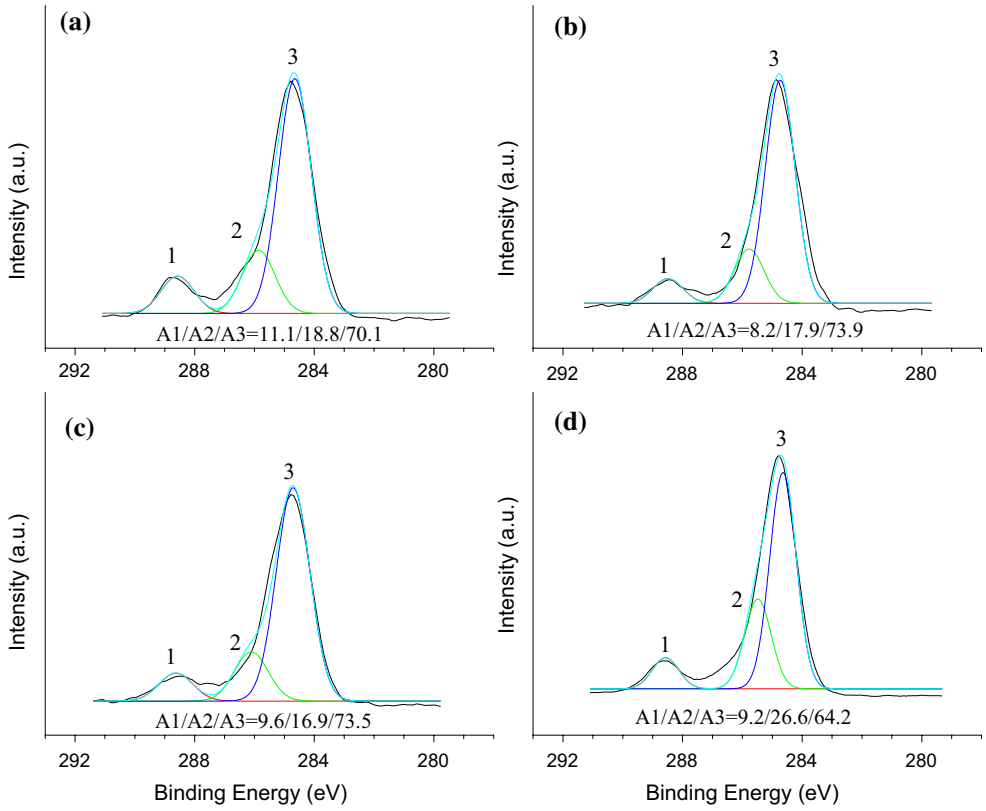

Fig. 9 C1s XPS spectra on the worn surfaces with different diameter dimples: UT (**a**), TSD (**b**), TMD (**c**) and TLD (**d**)

and iron oxide [41–43], respectively. The absence of peaks at ~ 706.7 eV indicates that all the rubbing surfaces are covered by adsorbed layers and a tribo-film [44]. The main antiwear components in the lubricating film were ferrous sulfide and iron hydroxide, which might help to reduce wear [45, 46]. Although there is a relatively large peak for iron hydroxide for the UT sample, the total concentration of the iron is the lowest. Thus, the contents of the main antiwear components for the UT surfaces are the lowest, resulting in the greater wear. For the worn surfaces of the TLD sample, the iron oxides had the largest component, indicating that textured surfaces with large-diameter dimples destroyed the continuity of the lubricating film and formed the oxides [47]. The positive effect of these tribo-oxide components is that they can firmly combine on the worn surfaces which make for the better antiwear properties of the TLD than those of the others. Additionally, a relative contribution of the peak at ~ 712.1 eV for the worn surfaces of TSD and TLD samples suggests a high content of ferrous sulfate [48]. The low lubricity of the ferrous sulfate [49] accounts for the higher friction coefficient of the TLD sample than that of the UT [50]. However, with the help of the lubricating oil film, the TSD surfaces still maintain a relatively low friction coefficient.

Figure 12 shows the S2p XPS spectra of the worn textured surfaces with different diameter dimples. The peaks at ~ 168.6 and ~ 160.1 eV can be assigned to the sulfates and sulfides [51, 52], respectively, originating from the base oil. There was a relatively higher content of iron sulfate on the TLD samples, in accord with the results in Fig. 11, and resulted in higher friction. Meanwhile, a higher content of iron sulfides was helpful for both anti-friction and antiwear [53]. This caused all the textured surfaces to have a lower wear volume than the UT surfaces. It seems like a contradiction since the total sulfur content on the worn surfaces and iron sulfides in the tribo-film of the TLD sample is the lowest, but it had a lowest wear volume. It can be explained by the fact that higher content of the other antiwear components such as tribo-oxide layer protects the textured surfaces, causing a light wear.

The content of typical elements on the worn surfaces of the UT and the textured surfaces with different density dimples is shown in Table 3. The worn surfaces may also have been covered by organics from the base oil since the carbon and oxygen dominated the components. After texturing, the iron content of all samples clearly increased. The content of iron and oxygen on the textured samples is higher than for the UT surfaces, indicating a thicker

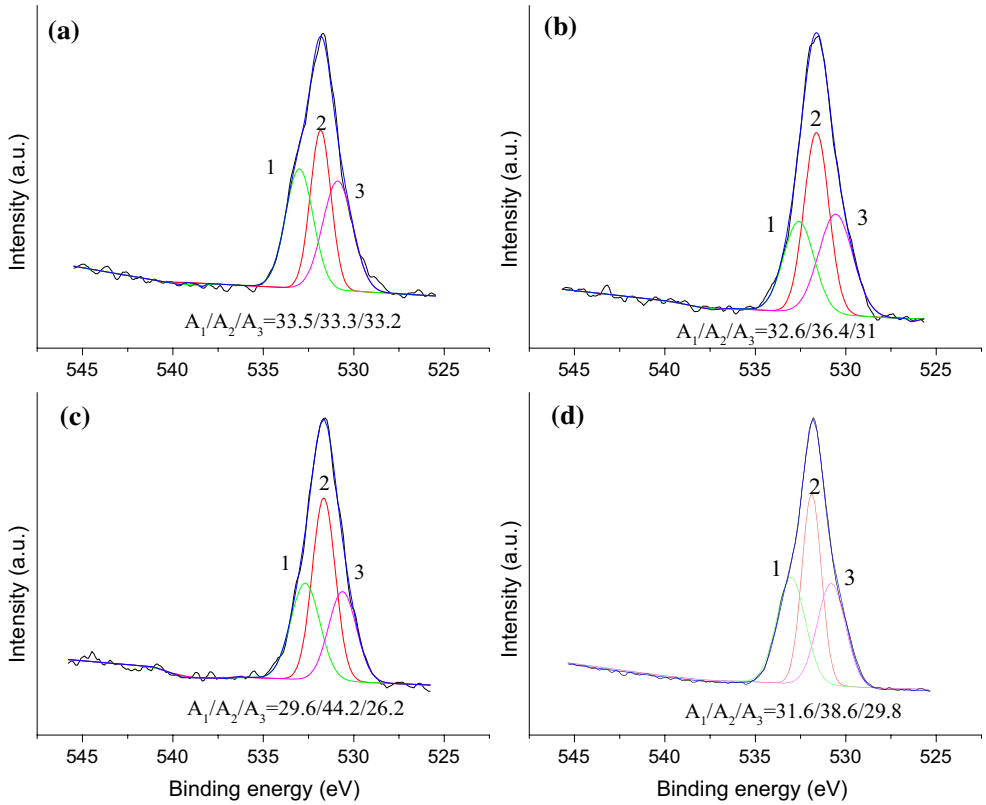

Fig. 10 O1s XPS spectra on the worn surfaces with different diameter dimples: UT (**a**), TSD (**b**), TMD (**c**) and TLD (**d**)

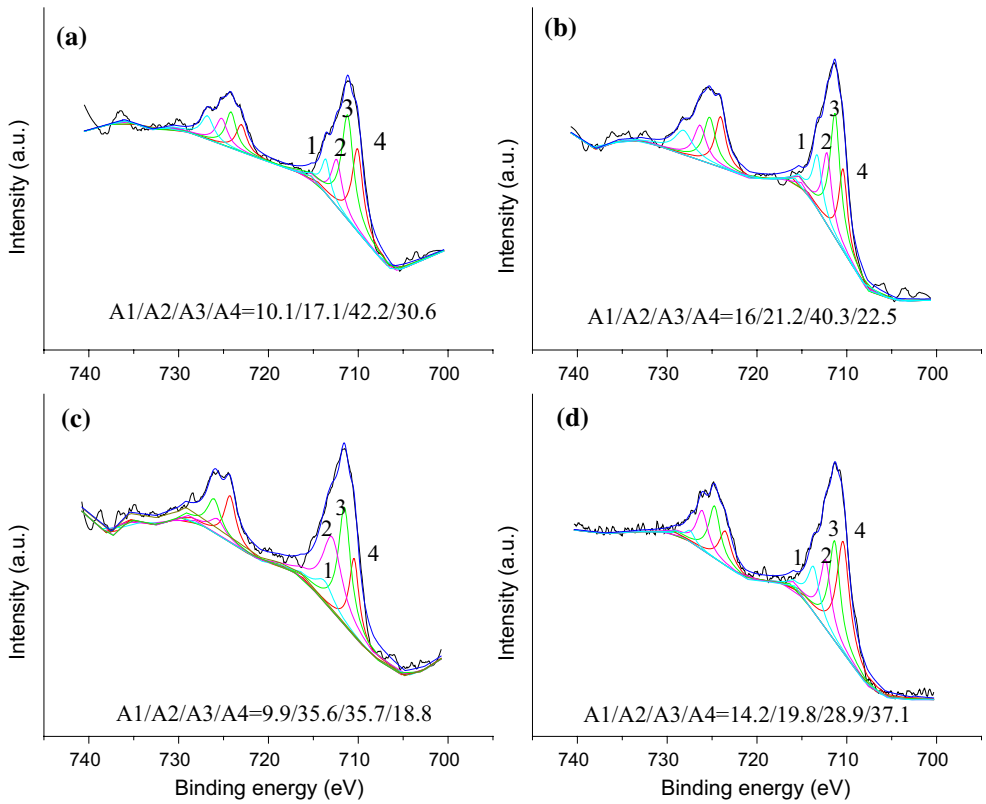

Fig. 11 Fe2p XPS spectra on the worn surfaces with different diameter dimples: UT (**a**), TSD (**b**), TMD (**c**) and TLD (**d**)

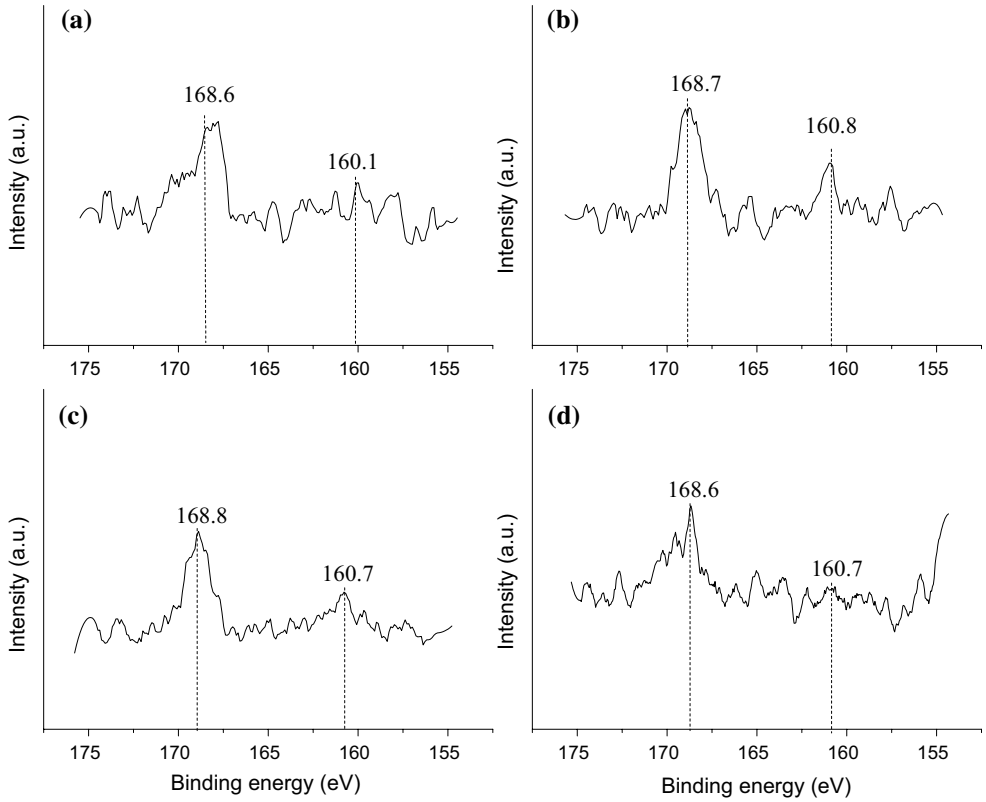

Fig. 12 S2p XPS spectra on the worn surfaces with different diameter dimples: UT (**a**), TSD (**b**), TMD (**c**) and TLD (**d**)

Table 3 The content of typical elements on the worn surfaces with different density dimples

The lower sample surfaces	Atomic percent (%)					
	Si	S	Mn	Fe	C	O
UT	2.36	1.46	0.86	1.98	69.43	23.91
TSLD	3.22	3.47	1.45	5.16	62.41	24.29
TMD	2.21	1.1	1.27	4.52	65.76	25.13
TSHD	4.14	2.42	2.28	4.98	61.19	25

tribo-oxide film on the textured surfaces. The protective role of this layer makes for less wear of the textured surfaces than the UT surfaces.

The C1s XPS spectra of the worn surfaces with different density dimples, shown in Fig. 13, indicate that the content of hydrocarbon on the worn surfaces decreased with the increase in the density of the dimples. Comparing with TMD, the TSLD and TSHD sample both had a high concentration of alcohol groups but a lower concentration of esters, which might contribute to the higher friction coefficients of TSLD and TSHD sample since esters have good antifriction effects [54].

The O1s XPS spectra on the worn surfaces with different density dimples shown in Fig. 14 can be divided into three components located at ~ 532.5 (Peak 1), ~ 531.8 (Peak 2) and ~ 530.8 (Peak 3) eV, which again correspond to sulfates, hydroxides and iron oxide [37], respectively. Comparing with the results for the TMD sample in Fig. 10, TSLD and TSHD samples have higher sulfate peak areas. This is also confirmed by the Fe2p XPS spectra in Fig. 15 because there were relatively components for ferrous sulfate at ~ 712.1 eV on TSLD and TSHD surfaces. Meanwhile, the TSLD and TSHD samples had a smaller peak at ~ 711.9 eV than for TMD surfaces, suggesting that they had a lower content of ferrous sulfide, that is, a thinner or incomplete lubricating films. This might be one aspect leads to the higher friction coefficient of TSLD and TSHD than that of the UT surfaces.

The S2p peaks at ~ 168.2 and ~ 160.1 eV in Fig. 16 can again be ascribed to sulfates and sulfides, respectively, from the oil. The relatively higher peak areas of iron sulfates and

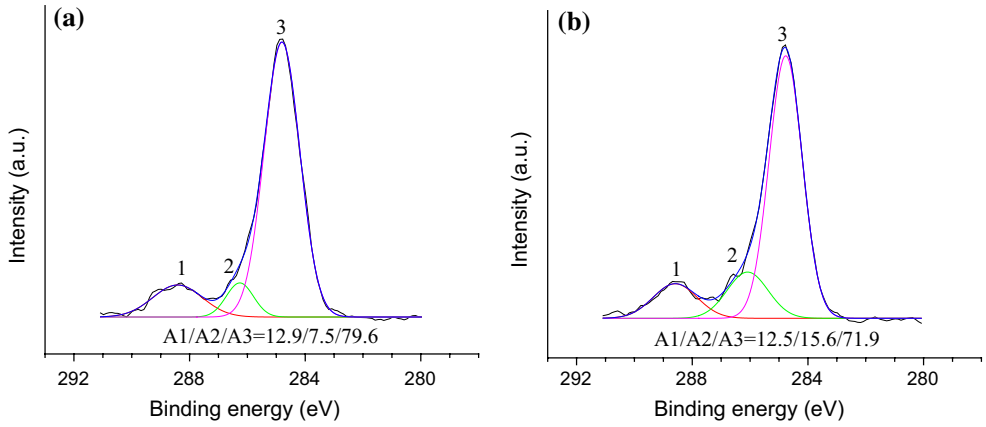

Fig. 13 C1s XPS spectra on the worn surfaces with different density dimples: TSLD (**a**), TSHD (**b**)

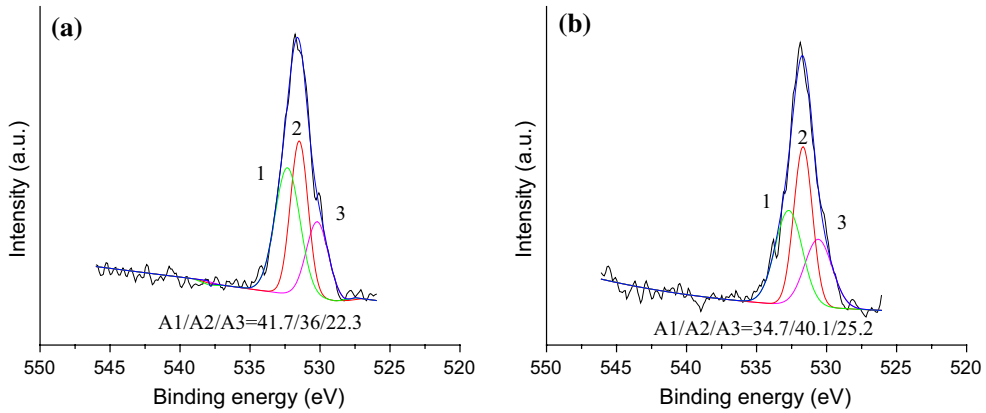

Fig. 14 O1s XPS spectra on the worn surfaces with different density dimples: TSLD (**a**), TSHD (**b**)

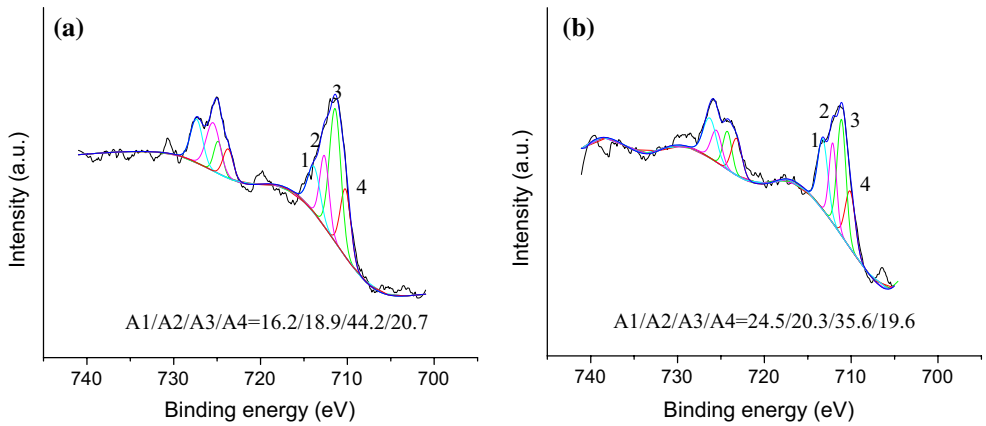

Fig. 15 Fe2p XPS spectra on the worn surfaces with different density dimples: TSLD (**a**), TSHD (**b**)

lower peak areas of iron sulfides of the TSLD and TSHD samples than those of TMD in Fig. 12 agree well with the results in Figs. 14 and 15. Another aspect is that the three-body abrasive role of the iron sulfates and deficiency of ferrous sulfides contribute to the higher friction coefficients of TSLD and TSHD compared to the TMD sample.

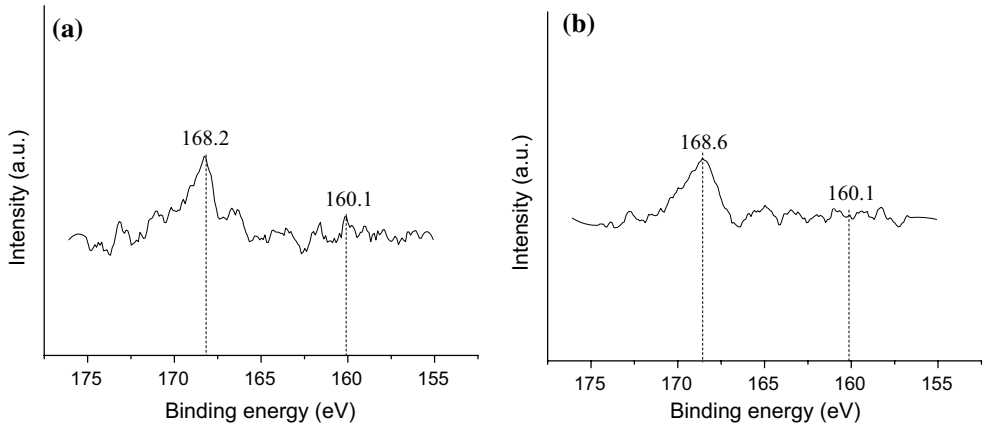

Fig. 16 S2p XPS spectra on the worn surfaces with different density dimples: TSLD (**a**), TSHD (**b**)

4 Conclusions

In the present work, a novel method for texturing steel surfaces using photolithographic etching was described and the tribological behavior was studied. It is apparent that photolithography etching can provide a simple and effective method for fabricating dimple arrays on steel samples. Comparing to the traditional laser texturing technology, the textured surfaces made by photolithography etching do not need further polishing. In addition, this approach has the advantage that it can easily be adapted to fabricate textured surfaces with different shapes, sizes and distributions by merely by changing the masks.

It was found that textured surfaces had a lower wear and lower friction coefficients than untextured (UT) surfaces except for the TLD surfaces, which had a higher friction coefficient. This could be due to the fact that the oil micro-reservoir and the ability of the dimples to contain wear debris contribute to forming a complete tribo-film and improving the friction and wear properties, but larger dimples destroyed the continuous oil film and increase the friction force.

An increase in the density of the dimples caused the wear of the textured surfaces to decrease and then increase at higher dimple densities. Both the TSLD and TSHD samples had higher friction than TMD and UT surfaces. This can be attributed to the presence of a thinner or incomplete lubricating oil film on the TSLD and TSHD surfaces due to the different density of the dimples. Thus, textured surfaces with appropriate diameters and densities present an opportunity to improve the friction and wear performance, which can be attributed to the combined effects of the formation of a complete and robust adsorbed and tribo-reacted film and the ability to contain the wear debris.

The differences of the tribological behavior and tribo-film of the photolithography etching surfaces and LST surfaces under the same conditions are worthy of being investigated further to illustrate their tribological mechanisms in the future.

Acknowledgements The authors appreciate Dr. Heather Adams and Mr. Xavier Udad for their assistance in the surface texturing process, and the authors would like to thank Prof. Kunhong Hu and Dr. Enzhu Hu for their help in the tribo-tests. This work was supported by the National Natural Science Foundation of China (Grant No. 51405124).

References

1. Wagner, J.J., Jenson, A.D., Sundararajan, S.: The effect of contact pressure and surface texture on running-in behavior of case carburized steel under boundary lubrication. Wear **376**, 851–857 (2017)
2. Etsion, I.: Modeling of surface texturing in hydrodynamic lubrication. Friction **1**, 195–209 (2013)
3. Brizmer, V., Kligerman, Y., Etsion, I.: A laser surface textured parallel thrust bearing. Tribol. Trans. **46**, 397–403 (2003)
4. Kovalchenko, A., Erdemir, A., Ajayi, O., Etsion, I.: Tribological behavior of oil-lubricated laser textured steel surfaces in conformal flat and non-conformal contacts. Mater. Perform. Charact. **6**, 1–23 (2017)
5. Taee, M., Torabi, A., Akbarzadeh, S., Khonsari, M., Badrossamay, M.: On the performance of EHL contacts with textured surfaces. Tribol. Lett. **65**, 85 (2017)
6. Sedlaček, M., Podgornik, B., Ramalho, A., Česnik, D.: Influence of geometry and the sequence of surface texturing process on tribological properties. Tribol. Int. **115**, 268–273 (2017)
7. Su, B., Huang, L., Huang, W., Wang, X.: The load carrying capacity of textured sliding bearings with elastic deformation. Tribol. Int. **109**, 86–96 (2017)
8. Chae, Y.H.: Effect of size for micro-scale dimples on surface under lubricated sliding contact. Key Eng. Mater. **345–346**, 765–768 (2007)

9. Etsion, I., Halperin, G., Brizmer, V., Kligerman, Y.: Experimental investigation of laser surface textured parallel thrust bearings. Tribol. Lett. **17**, 295–300 (2004)
10. Yu, H., Wang, X., Zhou, F.: Geometric shape effects of surface texture on the generation of hydrodynamic pressure between conformal contacting surfaces. Tribol. Lett. **37**, 123–130 (2010)
11. Etsion, I.: State of the art in laser surface texturing. In: Luo, J., Meng, Y., Shao, T., Zhao, Q. (eds.) Advanced Tribology, pp. 761–762. Springer, Heidelberg (2009)
12. Etsion, I., Sher, E.: Improving fuel efficiency with laser surface textured piston rings. Tribol. Int. **42**, 542–547 (2009)
13. Pettersson, U., Jacobson, S.: Influence of surface texture on boundary lubricated sliding contacts. Tribol. Int. **36**, 857–864 (2003)
14. Ye, J., Zhang, H., Liu, X., Liu, K.: Low wear steel counterface texture design: a case study using micro-pits texture and alumina–PTFE nanocomposite. Tribol. Lett. **65**, 165 (2017)
15. Daniel, C., Manderla, J., Hallmann, S., Emmelmann, C.: Influence of an angular hatching exposure strategy on the surface roughness during picosecond laser ablation of hard materials. Phys. Procedia **83**, 135–146 (2016)
16. Hu, J., Xu, H.: Friction and wear behavior analysis of the stainless steel surface fabricated by laser texturing underwater. Tribol. Int. **102**, 371–377 (2016)
17. Saeidi, F., Parlinska-Wojtan, M., Hoffmann, P., Wasmer, K.: Effects of laser surface texturing on the wear and failure mechanism of grey cast iron reciprocating against steel under starved lubrication conditions. Wear **386–387**, 29–38 (2017)
18. Touche, T., Cayer-Barrioz, J., Mazuyer, D.: Friction of textured surfaces in ehl and mixed lubrication: effect of the groove topography. Tribol. Lett. **63**, 25 (2016)
19. Xu, S., Shimada, K., Mizutani, M., Kuriyagawa, T.: Fabrication of hybrid micro/nano-textured surfaces using rotary ultrasonic machining with one-point diamond tool. Int. J. Mach. Tools Manuf. **86**, 12–17 (2014)
20. Kawasegi, N., Ozaki, K., Morita, N., Nishimura, K., Yamaguchi, M.: Development and machining performance of a textured diamond cutting tool fabricated with a focused ion beam and heat treatment. Precis. Eng. **47**, 311–320 (2017)
21. Holmes, P., Snell, J.: A vapour etching technique for the photolithography of silicon dioxide. Microelectron. Reliab. **5**, 337–341 (1966)
22. Atar, G., Ternyak, O., Greental, D., Eger, D., Chechelnitsky, G., Mazurski, N., et al.: Fabrication and characterization of large-core Yb/Al-codoped fused silica waveguides using dry etching. Opt. Mater. **38**, 265–271 (2014)
23. Zhang, J., Meng, Y.: A study of surface texturing of carbon steel by photochemical machining. J. Mater. Process. Technol. **212**, 2133–2140 (2012)
24. Costa, H., Hutchings, I.: Hydrodynamic lubrication of textured steel surfaces under reciprocating sliding conditions. Tribol. Int. **40**, 1227–1238 (2007)
25. Gachot, C., Rosenkranz, A., Hsu, S.M., Costa, H.L.: A critical assessment of surface texturing for friction and wear improvement. Wear **372**, 21–41 (2017)
26. Braun, D., Greiner, C., Schneider, J., Gumbsch, P.: Efficiency of laser surface texturing in the reduction of friction under mixed lubrication. Tribol. Int. **77**, 142–147 (2014)
27. Li, K., Yao, Z., Hu, Y., Gu, W.: Friction and wear performance of laser peen textured surface under starved lubrication. Tribol. Int. **77**, 97–105 (2014)
28. Zhang, H., Ding, B., Chen, T.: A high efficiency industrial polysilicon solar cell with a honeycomb-like surface fabricated by wet etching using a photoresist mask. Appl. Surf. Sci. **387**, 1265–1273 (2016)
29. Pettersson, U., Jacobson, S.: Friction and wear properties of micro textured DLC coated surfaces in boundary lubricated sliding. Tribol. Lett. **17**, 553–559 (2004)
30. Xiong, D., Qin, Y., Li, J., Wan, Y., Tyagi, R.: Tribological properties of PTFE/laser surface textured stainless steel under starved oil lubrication. Tribol. Int. **82**, 305–310 (2015)
31. Xie, M., Tang, H., Yao, H.: Failure analysis of tire separation in two-sized tires on Airbus planes. Eng. Fail. Anal. **61**, 21–27 (2016)
32. Zheng, X., Xu, Y., Geng, J., Peng, Y., Olson, D., Hu, X.: Tribological behavior of Fe_3O_4/MoS_2 nanocomposites additives in aqueous and oil phase media. Tribol. Int. **102**, 79–87 (2016)
33. Xu, Y., Peng, Y., Dearn, K.D., You, T., Geng, J., Hu, X.: Fabrication and tribological characterization of laser textured boron cast iron surfaces. Surf. Coat. Technol. **313**, 391–401 (2017)
34. Yu, H., He, J., Sun, L., Tanaka, S., Fugetsu, B.: Influence of the electrochemical reduction process on the performance of graphene-based capacitors. Carbon **51**, 94–101 (2013)
35. Bordes, A., Eom, K., Fuller, T.F.: The effect of fluoroethylene carbonate additive content on the formation of the solid-electrolyte interphase and capacity fade of Li-ion full-cell employing nano Si–graphene composite anodes. J. Power Sources **257**, 163–169 (2014)
36. Zhou, J.G., Thompson, J., Cutler, J., Blyth, R., Kasrai, M., Bancroft, G.M., et al.: Resolving the chemical variation of phosphates in thin ZDDP tribofilms by X-ray photoelectron spectroscopy using synchrotron radiation: evidence for ultraphosphates and organic phosphates. Tribol. Lett. **39**, 101–107 (2010)
37. Bhattacharya, P., Nandasiri, M.I., Lv, D., Schwarz, A.M., Darsell, J.T., Henderson, W.A., et al.: Polyamidoamine dendrimer-based binders for high-loading lithium–sulfur battery cathodes. Nano Energy **19**, 176–186 (2016)
38. Su, L., Hei, J., Wu, X., Wang, L., Zhou, Z.: Ultrathin layered hydroxide cobalt acetate nanoplates face-to-face anchored to graphene nanosheets for high-efficiency lithium storage. Adv. Funct. Mater. **27**, 1605544 (2017)
39. De Bonis, A., Lovaglio, T., Galasso, A., Santagata, A., Teghil, R.: Iron and iron oxide nanoparticles obtained by ultra-short laser ablation in liquid. Appl. Surf. Sci. **353**, 433–438 (2015)
40. Blanco, D., González, R., Viesca, J., Fernández-González, A., Bartolomé, M., Battez, A.H.: Antifriction and antiwear properties of an ionic liquid with fluorine-containing anion used as lubricant additive. Tribol. Lett. **65**, 66 (2017)
41. Strauss, E., Ardel, G., Livshits, V., Burstein, L., Golodnitsky, D., Peled, E.: Lithium polymer electrolyte pyrite rechargeable battery: comparative characterization of natural pyrite from different sources as cathode material. J. Power Sources **88**, 206–218 (2000)
42. Ferris, F., Tazaki, K., Fyfe, W.: Iron oxides in acid mine drainage environments and their association with bacteria. Chem. Geol. **74**, 321–330 (1989)
43. Xu, Y., Peng, Y., Zheng, X., Wang, H., Hu, X.: Influence of microalgal bio-oil on the lubrication properties of engine oil. Oil Gas Sci. Technol. **71**, 29 (2016)
44. Minfray, C., Martin, J., De Barros, M., Le Mogne, T., Kersting, R., Hagenhoff, B.: Chemistry of ZDDP tribofilm by ToF-SIMS. Tribol. Lett. **17**, 351–357 (2004)
45. You, Y.-L., Li, D.-X., Si, G.-J., Deng, X.: Investigation of the influence of solid lubricants on the tribological properties of polyamide 6 nanocomposite. Wear **311**, 57–64 (2014)
46. Loehlé, S., Matta, C., Minfray, C., Le Mogne, T., Iovine, R., Obara, Y., et al.: Mixed lubrication of steel by C18 fatty acids revisited. Part II: influence of some key parameters. Tribol. Int. **94**, 207–216 (2016)
47. Qi, X., Ma, J., Jia, Z., Yang, Y., Gao, H.: Effects of weft density on the friction and wear properties of self-lubricating fabric liners for

journal bearings under heavy load conditions. Wear **318**, 124–129 (2014)
48. Xian, Y., Wang, Y., Wen, S., Nie, Q., Deng, J.: Floatability and oxidation of pyrite with different spatial symmetry. Miner. Eng. **72**, 94–100 (2015)
49. Patel, M., Aswath, P.: Role of thermal, mechanical and oxidising treatment on structure and chemistry of carbon black and its impact on wear and friction Part I: extreme pressure condition. Tribol. Mater. Surf. Interfaces **9**, 1–18 (2015)
50. Baldwin, B.A.: Relationship between surface composition and wear: an X-ray photoelectron spectroscopic study of surfaces tested with organosulfur compounds. ASLE Trans. **19**, 335–344 (1976)
51. Fantauzzi, M., Elsener, B., Atzei, D., Rigoldi, A., Rossi, A.: Exploiting XPS for the identification of sulfides and polysulfides. RSC Adv. **5**, 75953–75963 (2015)
52. Barros, M.I.D., Bouchet, J., Raoult, I., Mogne, T.L., Martin, J.M., Kasrai, M., et al.: Friction reduction by metal sulfides in boundary lubrication studied by XPS and XANES analyses. Wear **254**, 863–870 (2003)
53. Zhou, L.H., Wei, X.C., Ma, Z.J., Mei, B.: Anti-friction performance of FeS nanoparticle synthesized by biological method. Appl. Surf. Sci. **407**, 21–28 (2017)
54. Singh, R.K., Gupta, P., Sharma, O.P., Ray, S.S.: Homogeneous synthesis of cellulose fatty esters in ionic liquid (1-butyl-3-methylimidazolium chloride) and study of their comparative antifriction property. J. Ind. Eng. Chem. **24**, 14–19 (2015)